PERGAMON

Journal of Structural Geology 25 (2003) 703–715

JOURNAL OF STRUCTURAL GEOLOGY

www.elsevier.com/locate/jstrugeo

Solution slip and separations on strike-slip fault zones: theory and application to the Mattinata Fault, Italy

Andrea Billi*

Dipartimento di Scienze Geologiche, Università "Roma Tre", Largo S. L. Murialdo 1, 00146, Rome, Italy

Received 25 July 2001; accepted 30 May 2002

Abstract

We present a set of relationships to determine the component of slip and separations generated by the cleavage-controlled volume contraction in strike-slip fault zones. The fault walls can translate toward each other along the (cleavage-normal) axis of maximum shortening as rock is dissolved by pressure solution along patterned cleavage surfaces within strike-slip fault zones. The fault zone shortening produces an 'apparent slip' and possible separations of reference stratigraphic surfaces across the fault zone. Solution related slip and separations can differ in magnitude and have either the same or the opposite sense. These discrepancies depend upon the amount of fault zone shortening and upon the angles between the fault and the shortening axis, and between the fault and the reference stratigraphic surface. Separations can be considerable at any scales even for very low amounts of fault zone thinning. Apparent slip can be appreciable for large amounts of fault zone thinning and/or high fault-to-cleavage incidence angles. With the proper geometrical conversions, the relationships here presented can apply to any fault type.

The application of this technique to the left-lateral Mattinata Fault, Italy, demonstrated that both left- and right-lateral strike separations can occur along the fault even for low amounts of fault zone contraction by rock dissolution.

Keywords: Solution slip; Solution separation; Solution cleavage; Fault zone shortening; Mattinata Fault

1. Introduction

The development of cleavage surfaces by pressure solution (e.g. Sharpe, 1847; Durney, 1972) has long been recognised as a mechanism that can account for a large part of strain by material removal across faults (e.g. Mitra et al., 1984; Nickelsen, 1986; Wojtal and Mitra, 1986; Aydin, 1988; Peacock and Sanderson, 1995; Willemse et al., 1997; Billi and Salvini, 2000, 2001) or across broader regions of deformation (e.g. Groshong, 1975b, 1976; Engelder and Geiser, 1979; Wright and Henderson, 1992; Gray and Mitra, 1993; Durney and Kisch, 1994; Mitra, 1994; Markley and Wojtal, 1996; McNaught and Mitra, 1996; Davidson et al., 1998; Whitaker and Bartholomew, 1999). Rock dissolution can result in a volume loss from minimum percentages (Wintsch et al., 1991), owing to the scarcity of water circulation (Engelder, 1984), up to 20% (Ramsay and Wood, 1972) and even 50–60% (Mimran, 1977; Alvarez et al., 1978; Wright and Platt, 1982; Beutner and Charles, 1985; Wright and Henderson, 1992).

Understanding magnitude, direction and sense of both slip and separation (*sensu* Dennis, 1967) on faults is commonly complicated by deceptive patterns created by the interaction between the attitudes of faults, stratigraphic surfaces and topography (e.g. Hobbs et al., 1976; Marshak and Mitra, 1988). Separations on faults in two-dimensional views (e.g. maps, cross-sections or outcrops) may be fully incongruent with fault slip by both magnitude and sense (Fig. 1). Thinning of exposure- to regional-scale fault zones by rock dissolution across solution cleavages may add components to fault slip and separations (Fig. 2). These additional components can be detected on two-dimensional views at the proper observation scales. The process invoked for the fault zone shortening is analogous to the well-known mechanism of truncation and offset of fossils and/or planar markers across single solution surfaces (e.g. Conybeare, 1949; Nickelsen, 1966; Groshong, 1975a; Bell, 1978; Roy, 1978).

In this paper, the components of fault slip and separations

* Tel.: +39-065-4888016; fax: +39-065-4888201.
E-mail address: billi@uniroma3.it (A. Billi).

0191-8141/02/$ - see front matter © 2002 Elsevier Science Ltd. All rights reserved.
PII: S0191-8141(02)00077-9

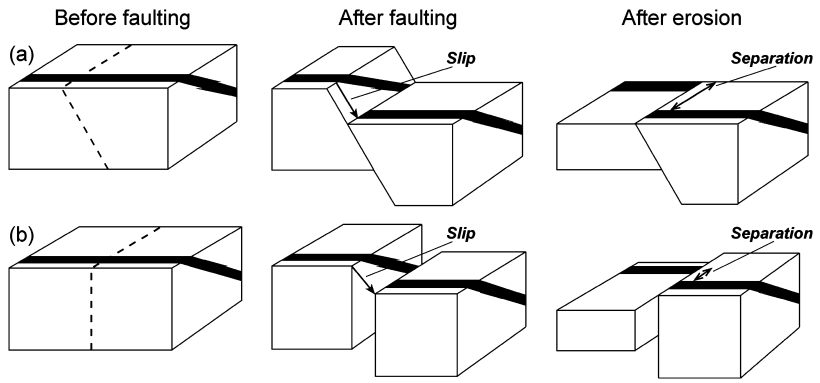

Fig. 1. Examples of discrepancies between slip and separations on erosion surfaces (modified after Hobbs et al., 1976). (a) Right-lateral separation parallel to strike of a fault developing by dip-slip displacement. (b) Right-lateral separation parallel to strike of a fault developing by oblique slip with left-lateral component.

generated by cleavage-controlled fault zone contraction are calculated for strike-slip fault zones, on the assumption that shortening occurs perpendicularly to solution cleavages. The method dealt with in this paper is of interest to those involved in the understanding of contradictory fault slip and separations along strike-slip faults in exposures, maps and cross-sections. Through simple geometrical rotations, this method can be applied to any fault zone type, within which shortening by cleavage-normal rock dissolution occurs.

2. Theory

2.1. Solution slip

Solution cleavage in strike-slip fault zones can develop as a continuous array of spaced, sub-parallel, solution surfaces within fault zones as wide as a few centimetres up to a few hundreds of metres (e.g. Nickelsen (1986) for thrusts, Peacock et al. (1999) and Salvini et al. (1999) for strike-slip faults). The cleavage to fault interceptions (Fig. 2) are usually vertical (i.e. in strike-slip fault zones) and parallel to the fault rotational axis that is an imaginary cylinder lying on the fault plane perpendicularly to the fault slicks and compelled to rotate congruously with the fault motion (Wise and Vincent (1965), geometrically coincident with the 'slip normal' of Wojtal (1986)). The cleavage surfaces can form with the fault an approximately constant angle (e.g. 40° in Salvini et al. (1999)). In such a fault zone, a contraction in volume by cleavage-normal rock dissolution (Nickelsen, 1972) generates an apparent slip (*sensu* Groshong, 1975a), *Sl* (Fig. 2), henceforth referred to as solution slip. This term applies to the along-strike component of the cleavage-normal shortening of the fault zone (Fig. 2). The relationship for *Sl* across the fault zone is:

$$Sl = \frac{Dn}{\tan(90^\circ - \alpha)} \quad (1)$$

in which *Dn* is the amount of fault-normal contraction and α is the angle from the cleavage to the fault, following the rotation sense of the fault rotational axis (Fig. 2).

The α angle may theoretically vary from 0 to 90°. In nature α is commonly around 45°, but may vary from a minimum of about 25° (i.e. transpressional shear zones) to a maximum of about 75° (i.e. transtensional shear zones) (van der Pluijm and Marshak, 1997). In Fig. 3 we plot the values of *Sl* against *Dn* for a theoretical fault zone 100 m in width ($W = 100$ m in Fig. 3) and for $\alpha = 25$, 50 and 75°. The diagram shows that *Sl* exceeds *W*, which can be taken as the resolution limit of observation, only for high values of *Dn* and α.

2.2. Solution separations

The fault zone contraction in volume can also produce stratigraphic separations (Fig. 2), henceforth referred to as solution separations.

2.2.1. Strike separation

The solution strike separation (i.e. the separation along the fault strike; Groshong, 1999), *Ps*, of a reference surface of stratigraphic nature depends upon the *Dn* magnitude, the fault to the stratigraphic surface angle (β), and the fault to the shortening axis (i.e. assumed as normal to the cleavage surfaces) angle (γ) that is equal to $90^\circ - \alpha$. The β and γ angles are measured, on the horizontal plane, starting from the fault plane and following the rotation sense of the fault rotational axis. β varies from 0 to 180°, whereas γ varies from 0 to 90°.

Ps for any inclined stratigraphic surface is calculated

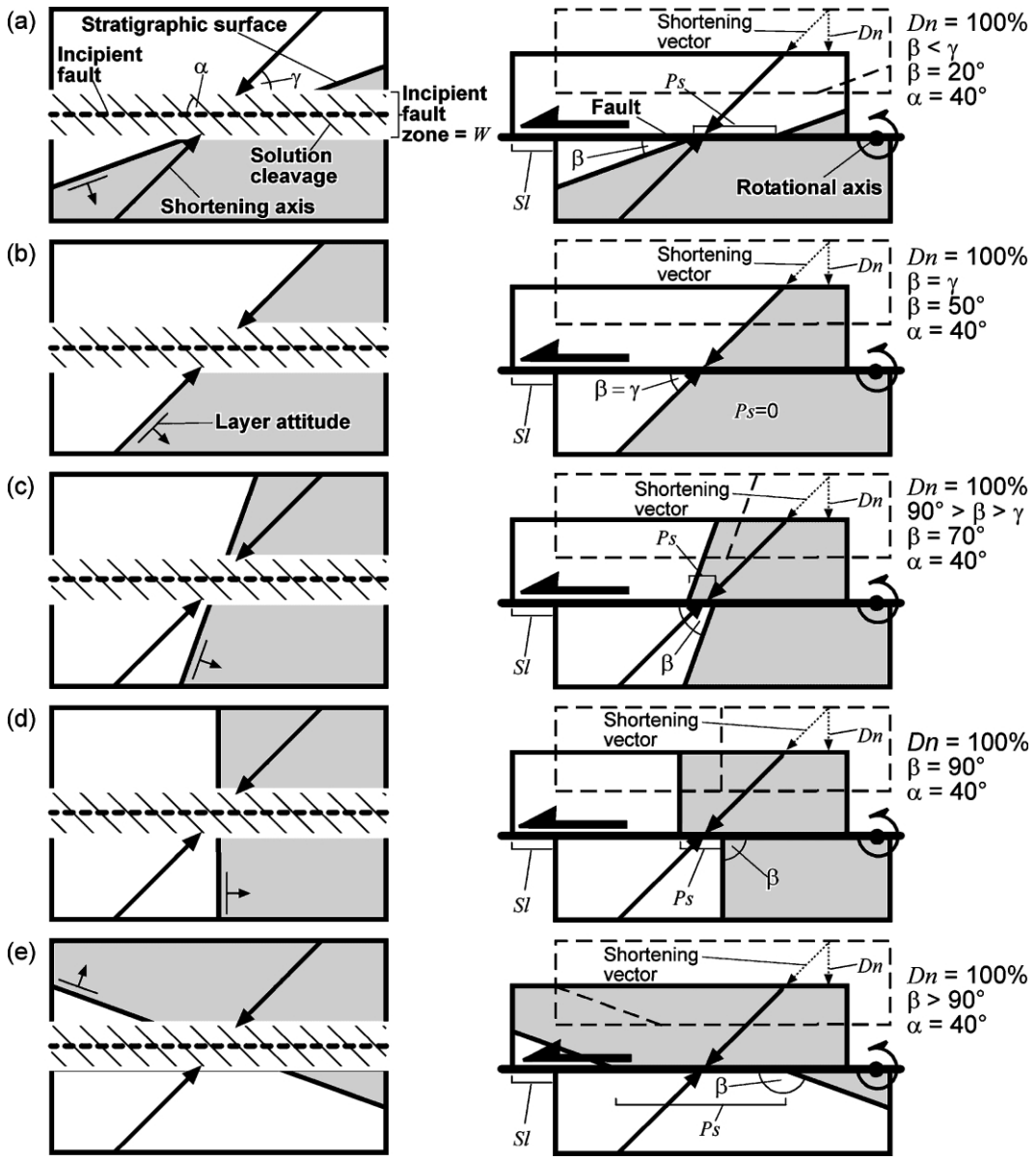

Fig. 2. Map views of left-lateral strike-slip fault zones developing across inclined marker surfaces. On the left, incipient fault zones with development of solution cleavages. Fault and solution cleavage surfaces are vertical. Their intersection lines are parallel to the fault rotational axis (see text for definition). On the right, the fault zones are removed by the rock dissolution across (i.e. normal to) the cleavage surfaces. The opposite fault blocks are translated towards each other along the cleavage-normal shortening axis. This process produces an apparent fault slip (solution slip or *Sl*) and different strike separations (solution strike separation or *Ps*) of the reference stratigraphic surface as a function of α and β angles. Note that in (a) *Sl* and *Ps* have opposite sense, in (b) *Ps* is equal to zero, and in (c)–(e) *Sl* and *Ps* have the same sense.

from the following expressions:

(a) for $\beta < \gamma$,

$$Ps = \frac{Dn}{\tan\beta} - Sl \tag{2}$$

(b) for $\beta = \gamma$,

$$Ps = 0 \tag{3}$$

(c) for $90° > \beta > \gamma$,

$$Ps = Sl - \frac{Dn}{\tan\beta} \tag{4}$$

(d) for $\beta = 90°$,

$$Ps = Sl \tag{5}$$

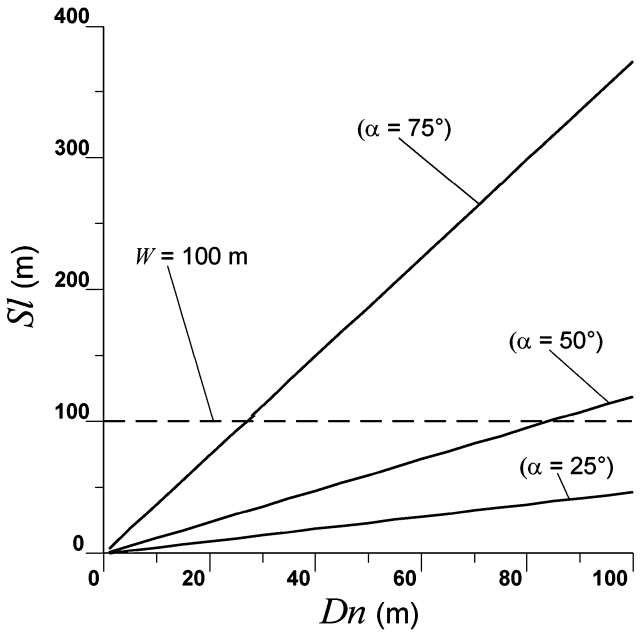

Fig. 3. Diagram of *Sl* vs. *Dn* for different α angles. *W* (= 100 m) is an hypothetical fault zone width plotted on the *y*-axis of the diagram. Note that taking the *W* as the resolution limit of observation, *Sl* exceeds this limit for high values of *Dn* and α.

(e) for $\beta > 90°$,

$$Ps = Sl + \frac{Dn}{\tan(180° - \beta)} \tag{6}$$

Sl and *Ps* have the same sense (Fig. 2c–e) for $\beta > \gamma$, and the opposite sense (Fig. 2a) for $\beta < \gamma$.

The *Sl* vs. β and *Ps* vs. β diagrams in Fig. 4a show that, in the case of a strike-slip fault zone 100 m in width, even for very low amounts of fault zone shortening (*Dn*), as β decreases below 20–30° or increases over 150–160°, the discrepancy in magnitude between *Sl* and *Ps* becomes significant and *Ps* exceeds the fault zone width (i.e. *W* in Fig. 4) that can be taken as the resolution limit of the observation scale. *Ps* positively (i.e. *Sl* and *Ps* have the same sense) increases with β decreasing below $180° - \gamma$, and negatively (i.e. *Sl* and *Ps* have the opposite sense) increases with β increasing over γ (Fig. 4a). *Ps* tends to infinity for β tending to 0° or 180°. *Sl* and *Ps* converge as β approaches 90°. The opposite sense of *Sl* and *Ps* depends upon the angular relationship between the reference stratigraphic surface and the shortening axis. *Sl* and *Ps* have opposite sense for the intersection line of the stratigraphic surface on the topographic surface falling between the fault and the shortening axis (Fig. 2a). *Sl* and *Ps* have the same sense for the intersection line of the stratigraphic surface on the topographic surface falling between the shortening axis and the fault (Fig. 2c–e). The discrepancy in magnitude between *Sl* and *Ps* increases as the angle between the fault and the stratigraphic surface (β) decreases.

2.2.2. Dip separation

The fault zone shortening by cleavage-normal rock dissolution can also produce a solution dip separation (i.e. the separation along the fault dip; Groshong, 1999), *Pd*, of any inclined stratigraphic surface (Fig. 5):

$$Pd = \frac{Dn}{\tan(90° - \delta)} \tag{7}$$

where δ is the dip of the stratigraphic surface as measured on the section normal to the fault strike (Fig. 5c).

Combining Eqs. (1) and (7) yields:

$$Sl = Pd\frac{\tan(90° - \delta)}{\tan(90° - \alpha)} \tag{8}$$

that allows calculating *Sl* from *Pd* and vice versa.

Pd increases with increasing *Dn* and δ and becomes appreciable (i.e. greater than *W* in Fig. 4b) for δ approaching 90°, even for very low *Dn* magnitudes (Fig. 4b). *Pd* is unrelated to β. Even for β equal to 0 or 180°, *Pd* has a nonzero magnitude.

2.2.3. Oblique separation

The fault zone shortening can also produce solution oblique separations (i.e. the separation on sections normal to the fault plane and oblique to the fault slip vector), *Pq*, of any inclined stratigraphic surface. *Pq* is calculated from the dip (ϵ) of the given section and from the dip (θ) of the reference stratigraphic surface as measured on the fault surface (Fig. 6). *Pq* on a section dipping to the same direction of the stratigraphic surface is:

(a) for $\epsilon > \theta$

$$Pq = \frac{Pd}{\sin(\epsilon - \theta)}\sin(90° + \theta) \tag{9}$$

(b) for $\epsilon < \theta$

$$Pq = \frac{Pd}{\sin(\theta - \epsilon)}\sin(90° - \theta) \tag{10}$$

(c) for $\epsilon = \theta$

$$Pq = 0 \tag{11}$$

whereas on a section dipping to the opposite direction of the stratigraphic surface,

$$Pq = \frac{Pd}{\sin(\theta + \epsilon)}\sin(90° - \theta) \tag{12}$$

Pq shows different magnitudes and opposite senses depending upon the attitude of the reference stratigraphic surface and the attitude of the given section (Fig. 4c). For synthetic ϵ and θ angles, *Pq*(Pq_s in Fig. 4b) tends to infinity as ϵ tends to θ, whereas for antithetic ϵ and θ angles, *Pq*

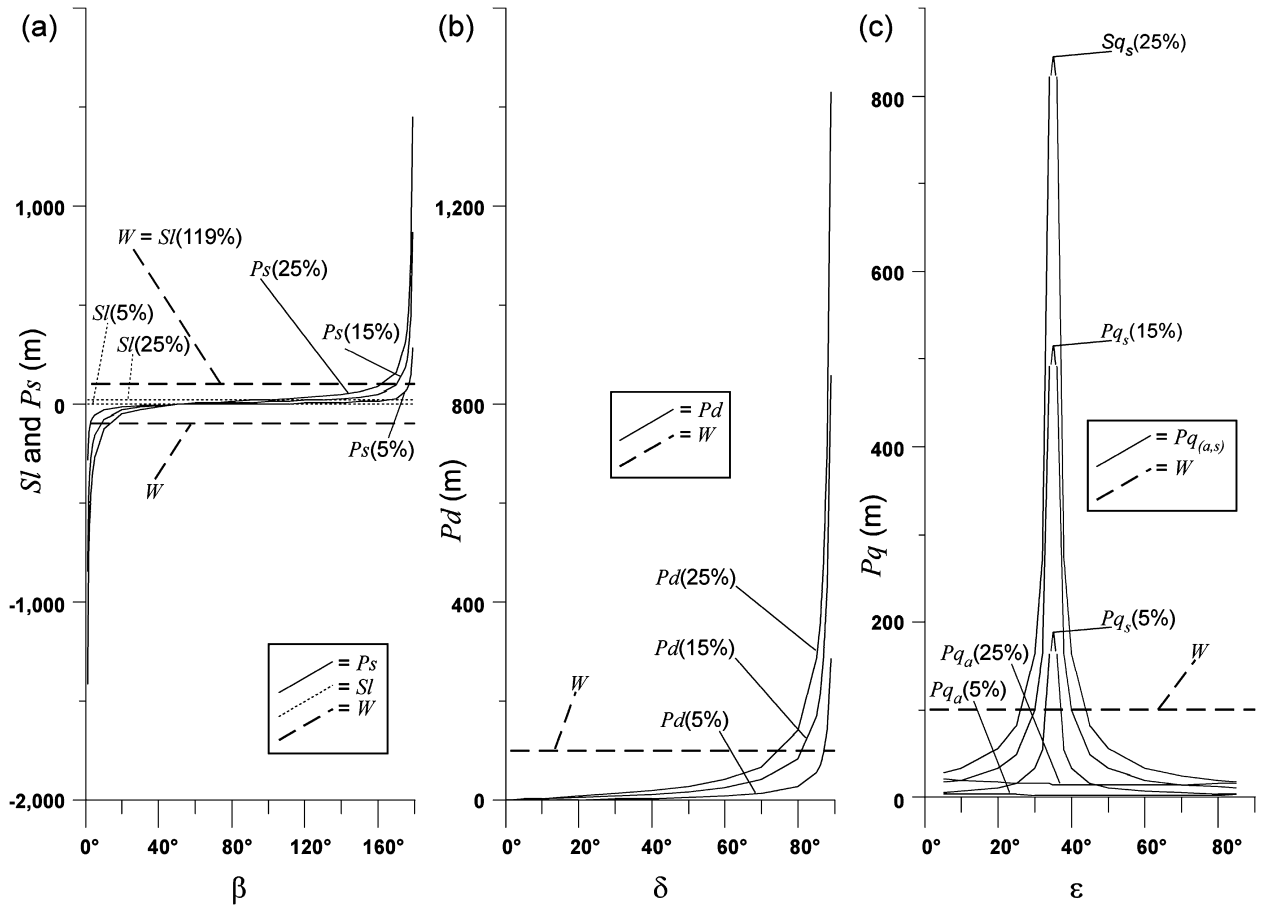

Fig. 4. Diagrams of solution separations (*Ps*, *Pd* and *Pq*) vs., respectively, β, δ, and ϵ. Separations are computed in the case of a strike-slip fault zone 100 m wide, $\alpha = 40°$, and *Dn* equal to 5, 15 and 25% of the fault zone width (100 m). *W* is the fault zone width plotted on the *y*-axis of the diagrams. (a) Diagram of *Sl* vs. β and *Ps* vs. β. Positive ordinates are for *Ps* with the same sense as *Sl*, negative ordinates are for *Ps* with opposite sense of *Sl*. Note that taking *W* as the resolution limit of observation, *Sl* is always under this limit. *Sl* would be equal to *W* for *Dn* equal to 119% of *W*. *Ps* may be up to 13–14 times *W* for *Dn* = 25% of *W*. (b) Diagram of *Pd* vs. δ. Note that *Pd* exceeds *W* for increasing δ and *Dn*. (c) Diagram of *Pq* vs. ϵ. Pq_s is the oblique separation measured on cross-sections dipping to the same direction of the index layer, Pq_a is the oblique separation measured on cross-sections dipping to the opposite direction.

(Pq_a in Fig. 4c) results under the resolution limit (*W* in Fig. 4c) even for large *Dn* magnitudes.

3. Application to the Mattinata Fault

3.1. Geological background

The Mattinata Fault (Fig. 7) in the Southern Apennines, Italy, is an E–W strike-slip fault (Funiciello et al., 1988) cutting through Meso-Cenozoic carbonate rocks of platform-to-slope origin (Bosellini et al., 1999). In the last decades, the Mattinata Fault has been the subject of several studies by both stratigraphers and structural geologists, who commented on the strike-slip kinematics of this fault (Ricchetti and Pieri, 1999, and reference therein). However, the sense of the strike-slip displacement on the Mattinata Fault is still the subject of a broad debate, owing to the contradictory stratigraphic separations (Fig. 7; Servizio Geologico d'Italia, 1965, 1970) and structural evidence (e.g. Salvini et al., 1999) along this fault. In summary, the Mattinata Fault and/or its eastward off-shore prolongation has been interpreted or mentioned as right-lateral (Guerricchio, 1983; 1986; Finetti and Del Ben, 1986; de Dominicis and Mazzoldi, 1987; Finetti et al., 1987; Doglioni et al., 1994; Tramontana et al., 1995; Anzidei et al., 1996; Morsilli and Bosellini, 1997; Guerricchio and Pierri, 1998; Bosellini et al., 1999), left-lateral (Funiciello et al., 1988; Favali et al., 1993; Salvini et al., 1999; Billi, 2000; Billi and Salvini, 2000; 2001), right- to left-lateral inverted (de Alteriis, 1995; Gambini and Tozzi, 1996), left- to right-lateral inverted (Chilovi et al., 2000), undetermined strike-slip (Aiello and de Alteriis, 1991; Bosellini et al., 1993a,b; Bertotti et al., 1999; Graziano, 1999; 2000; Casolari et al., 2000) or reverse (Ortolani and Pagliuca, 1987, 1988).

The Mattinata Fault (Fig. 8a) consists of a 200-m-wide, sub-vertical fault zone that cuts across carbonate beds that strike E–W (Fig. 8b) and dip southwards at 20–40°. Within the Mattinata Fault zone, a sub-vertical, closely-spaced solution cleavage developed for the entire length of the fault

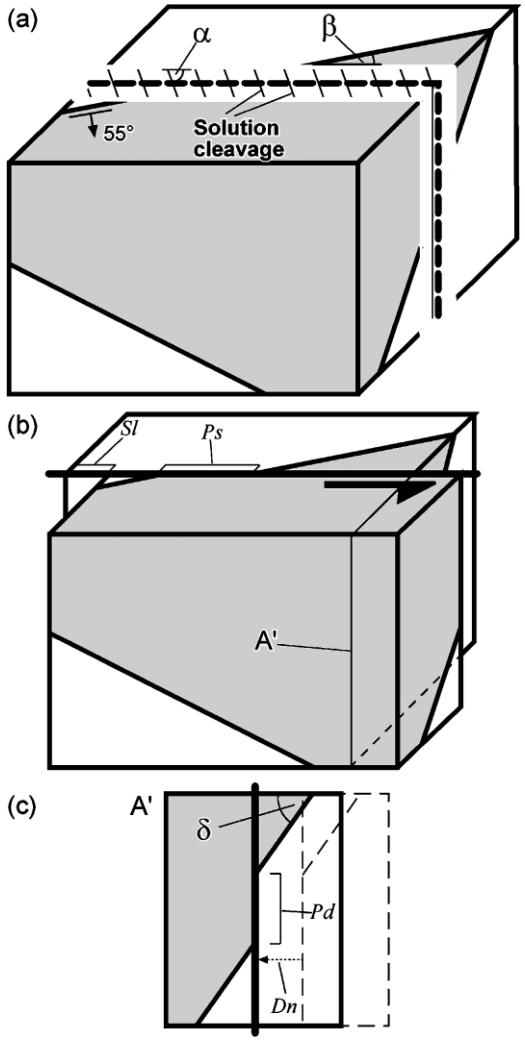

Fig. 5. (a) Block diagram of an inclined (dip = 55°) stratigraphic surface cut by a vertical, strike-slip fault zone with development of vertical solution cleavages. $\alpha = 40°$, $\beta = 20°$. (b) Same as (a), but the fault zone has been entirely removed by translating the two fault blocks towards each other along the cleavage-normal shortening axis. (c) Plan view of A′ cross-section in (b). A solution dip separation (Pd) of the stratigraphic surface can be observed on the cross-section at the proper observation scale.

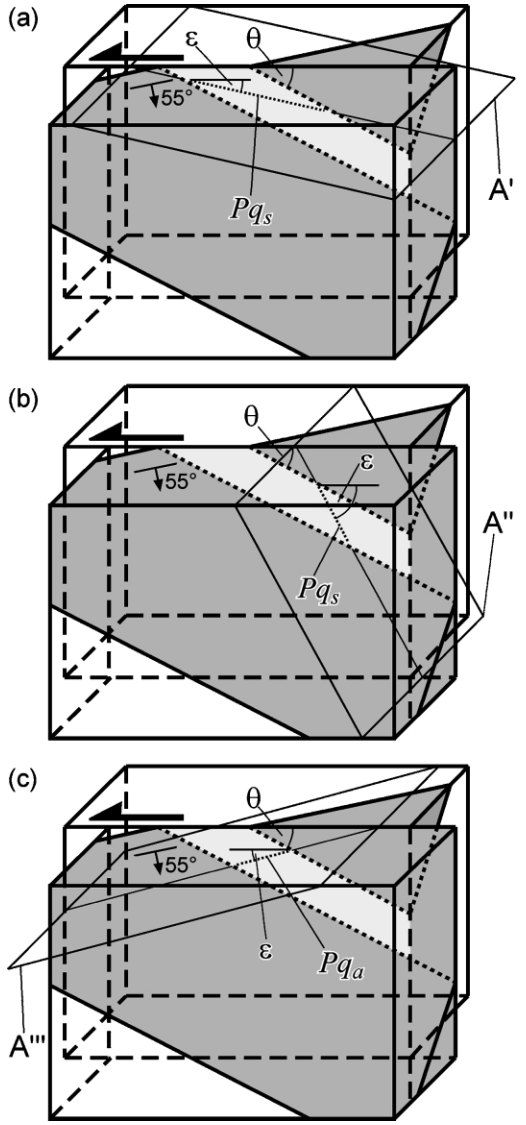

Fig. 6. Block diagrams showing a 55°-dipping stratigraphic surface cut by a vertical strike-slip fault. The fault zone has been entirely removed by translating the two fault blocks towards each other along the cleavage-normal shortening axis ($\alpha = 40°$). (a) Solution oblique separation (Pq_s) in the case of the stratigraphic surface and A′ section, in which the separation is computed, dipping to the same direction, with $\epsilon < \theta$. (b) Solution oblique separation (Pq_s) in the case of the stratigraphic surface and A″ section, in which the separation is computed, dipping to the same direction, with $\epsilon > \theta$. (c) Solution oblique separation (Pq_a) in the case of the stratigraphic surface and A‴ section, in which the separation is computed, dipping to the opposite directions.

with a NW–SE general trend (Fig. 8c). Cleavage surfaces form with the fault trace a rather constant α angle of 40° (Salvini et al., 1999). Cleavage consists of sinuous to planar surfaces with a wiggly to smooth profile (Fig. 9). Cleavage spacing measured perpendicular to cleavage surfaces is about 20 mm on average (Fig. 8d). Stylolite amplitude as measured on cleavage surface exposures is about 30 mm on average (Fig. 8e). No marker surfaces are known on both sides of the fault (Servizio Geologico d'Italia, 1965, 1970) except for the Mesozoic platform-to-slope margin exposed on the eastern side of the fault (Fig. 7). This surface is interpreted as a faulted (Masse and Luperto Sinni, 1987; Borgomano, 2000) and scalloped (Bosellini et al., 1993a,b) abrupt margin of the Mesozoic carbonate platform. In the southeastern Gargano Promontory, the Mattinata Fault cuts nearly parallel to this surface, which shows a strike separation on the fault of about 6000 m (S.S. in Fig. 7).

3.2. Solution slip and separations on the Mattinata Fault

By applying Eqs. (1)–(6) to the Mattinata Fault, we obtained an estimate of possible *Sl*s and *Ps*s along this fault (see Appendix A for the method of estimating equation

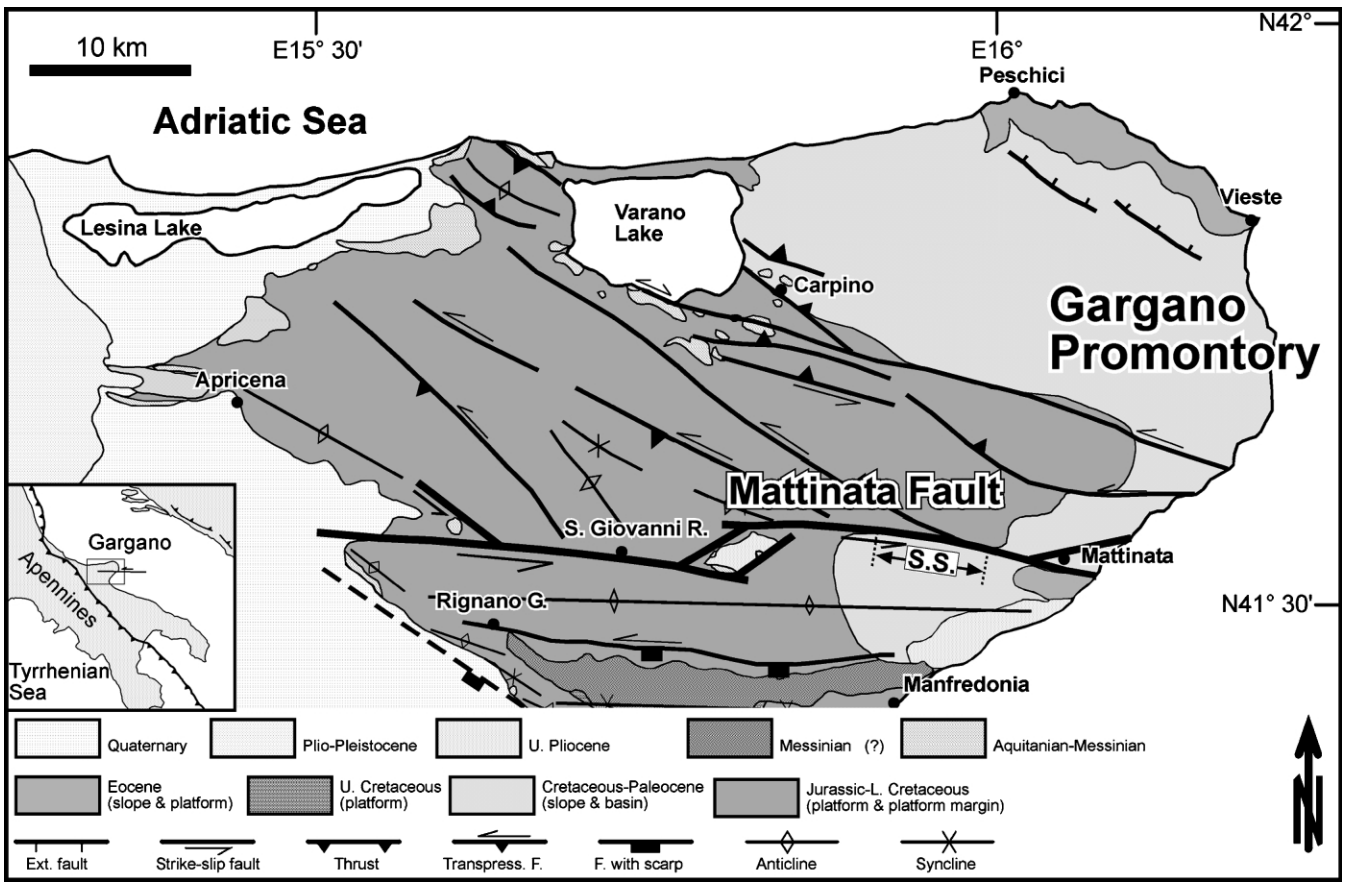

Fig. 7. Geological map of the Mattinata Fault area (modified after Servizio Geologico d'Italia (1965, 1970) and Casolari et al. (2000)). Note in the eastern portion of the Mattinata Fault the right-lateral strike separation (S.S. in the figure) of the platform-to-slope transition surface.

parameters and Table 1 in Appendix B for the input data). Results from this estimate are provided in Table 1 (Appendix B) and Fig. 10. *Sl* resulted as negligible in comparison with the fault zone size, since it varies from 6 to 30 m. By contrast, *Ps* was considerably greater than the fault zone size in places. In Fig. 10b, the Mattinata Fault trace as mapped on the 1:100,000 maps after Servizio Geologico d'Italia (1965, 1970) has been subdivided into 46 segments with strikes varying from N51°E to N118°E (Table 1 and Fig. 8a). For each segment, the computed *Ps* has been plotted as a function of the segment longitude at its median point (Fig. 10b). By assuming the fault zone width as the resolution limit (i.e. $W = 200$ m in Fig. 10b), *Ps* along the Mattinata Fault exceeds this limit both in the left- and in the right-lateral sense of slip. The maximum left-lateral value of *Ps* along the Mattinata Fault is 1015 m (Table 1, datum id = 19), whereas its maximum right-lateral value is 11,099 m (Table 1, datum id = 35). *Ps* in the eastern portion of the Mattinata Fault, where the fault cuts across the Mesozoic platform-to-slope boundary, varies from a minimum of 1025 m (Table 1, datum id = 36) to a maximum of 11,099 m (Table 1, datum id = 35) in the right-lateral sense (shaded area in Fig. 10b). The computed *Ps*s in the eastern portion of the Mattinata Fault can fully explain the 6000 m of right-lateral strike separation of the platform-to-slope boundary as mapped in Servizio Geologico d'Italia (1965, 1970) (Fig. 10a), even for an overestimate of *Dn* and apart from the fault mechanical translation whose magnitude is unknown. It should be borne in mind that these results are valid on the assumption of a nearly planar geometry of the platform-to-slope boundary surface, owing to its tectonic nature (e.g. Masse and Luperto Sinni, 1987; Tramontana et al., 1995). Conversely, the observed strike separation on the Mattinata Fault may simply be explained by the sinuous or even zigzag geometry that platform-to-slope boundaries may have (e.g. Sellwood, 1996).

4. Limits of the method

The method discussed above has limits on its application, which are worth discussing.

1. From Eq. (1) and Fig. 3 we infer that *Sl* should be commonly negligible with respect to mechanical translations along faults, unless the α angle is large and the

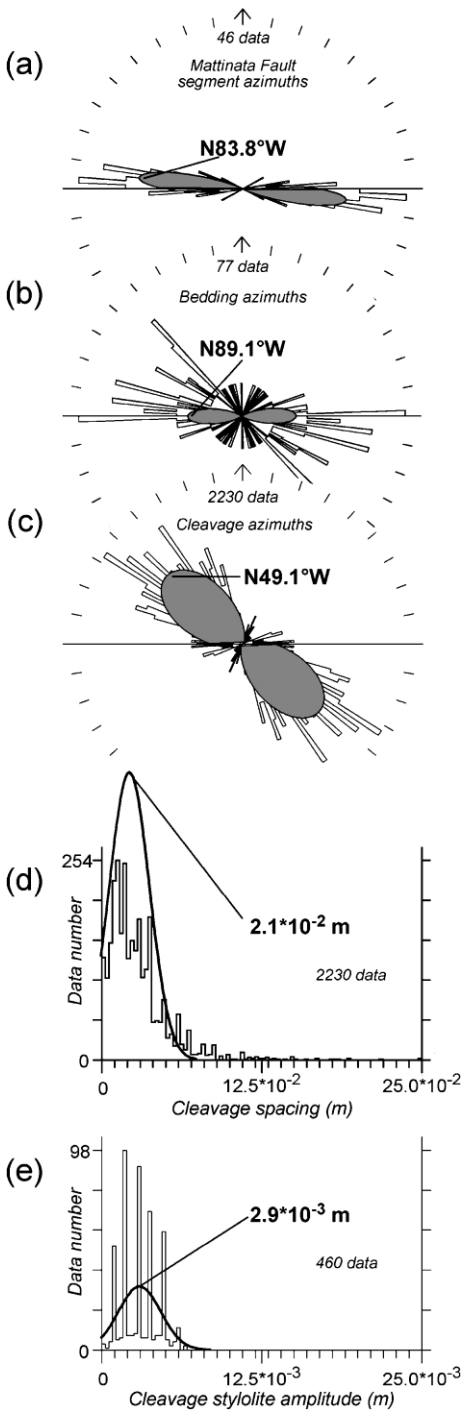

Fig. 8. (a) Histogram and Gaussian best fit of azimuths from the Mattinata Fault segments as digitised on 1:100,000 maps after Servizio Geologico d'Italia (1965, 1970). N84°W is the mean azimuth computed on the Gaussian best fit. (b) Histogram and Gaussian best fit of bedding azimuths as collected within a 2000-m-wide rectangular band encompassing the Mattinata Fault. N89.1°W is the mean azimuth computed on the Gaussian best fit. (c) Histogram and Gaussian best fit of cleavage azimuths as collected within the Mattinata Fault zone (data extracted after Salvini et al., 1999). N49°W is the mean azimuth computed on the Gaussian best fit. (d) Histogram and Gaussian best fit of cleavage spacing as collected within the Mattinata Fault zone (data extracted after Salvini et al., 1999). 21 mm is the mean cleavage spacing computed on the Gaussian best fit. (e) Histogram and Gaussian best fit of cleavage stylolite amplitude as collected within the Mattinata Fault zone. 2.9×10^{-3} 29 mm is the mean stylolite amplitude computed on the Gaussian best fit.

fault zone shortening by rock dissolution is rather high ($>15-20\%$ for $\alpha = 45°$), but these conditions have to be verified in nature. In the case of the Mattinata Fault, *Sl* should be at least one or two orders of magnitude smaller than the presumed mechanical translation that, on a first approximation, might be of the same order of the along strike dimension of the pull-apart basin located East of the S. Giovanni R. village (i.e. 2000 m; see also Ricchetti and Pieri, 1999, and reference therein).

2. As mentioned in the introductory section (Fig. 1), solution separations do not explain all observations of slip vs. separation discrepancies. Other explanations are possible for these discrepancies such as heterogeneous change of fault displacement associated with heterogeneous behaviour of the host rock, or the progressive decrease of the fault displacement at the ends of faults.
3. Fault zones that form through a combination of shear and volume reduction are known also in the absence of cleavage and rock dissolution (e.g. Aydin, 1978; Aydin and Johnson, 1978; Mollema and Antonellini, 1996). Volume reduction on these faults could generate 'apparent' slip and separations on the fault, which cannot be computed by the above-discussed method.

5. Conclusions

The method presented in this paper may partly explain the fault slip vs. separation discrepancies that can occur on maps, cross-sections and exposures. The assumption for the application of the method is that the fault zone contraction in volume occurs perpendicular to patterned fault-related cleavages such as those documented by Salvini et al. (1999). With simple geometrical rotations, this method may apply to fault types other than strike-slip.

Cleavage-controlled fault zone contraction can be at the origin of slip vs. separation discrepancies, in which stratigraphic separations along the same fault vary from the same to the opposite sense to the true slip. This, in particular, can occur for a reference stratigraphic surface sub-parallel to the fault zone, and intersecting it on both sides at small angles (e.g. Billi, 2000).

Acknowledgments

Comments and review by D. Peacock substantially improved this paper. The paper benefited also from constructive discussions with F. Rossetti, F. Salvini and F. Storti. M.C. Bertagnolio and E. Da Riva helped with the mathematics and 3D geometry. F. Salvini is thanked for kindly providing Daisy 2.0 software for structural analysis. The author wishes to thank two anonymous reviewers and T. Blenkinsop for insightful reviews.

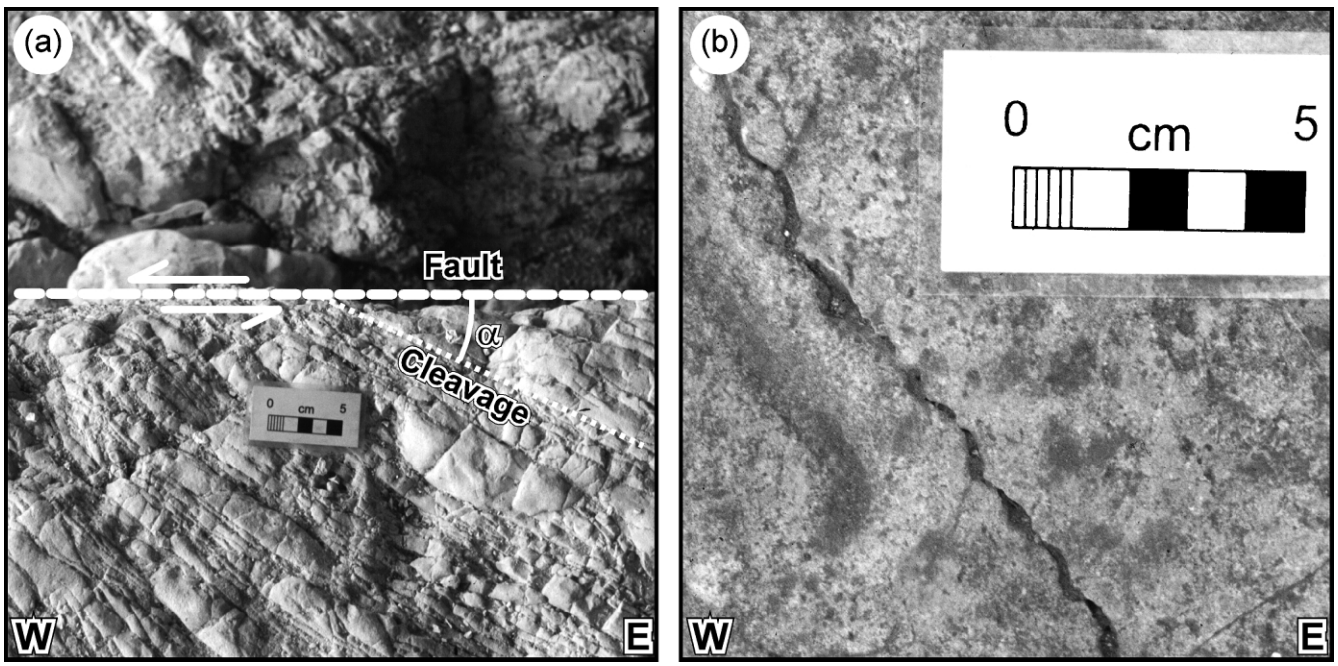

Fig. 9. (a) Photograph (map view) of an E–W left-lateral strike-slip fault (map view) cutting through NW–SE solution cleavage surfaces (Mattinata Fault zone, northeast of the Mattinata village). (b) Photograph (map view) of a bedding plane with the trace of a NW–SE subvertical solution cleavage surface (Mattinata Fault zone, east of the S. Giovanni Rotondo village). Note the undulating stylolitic profile with sinuous teeth.

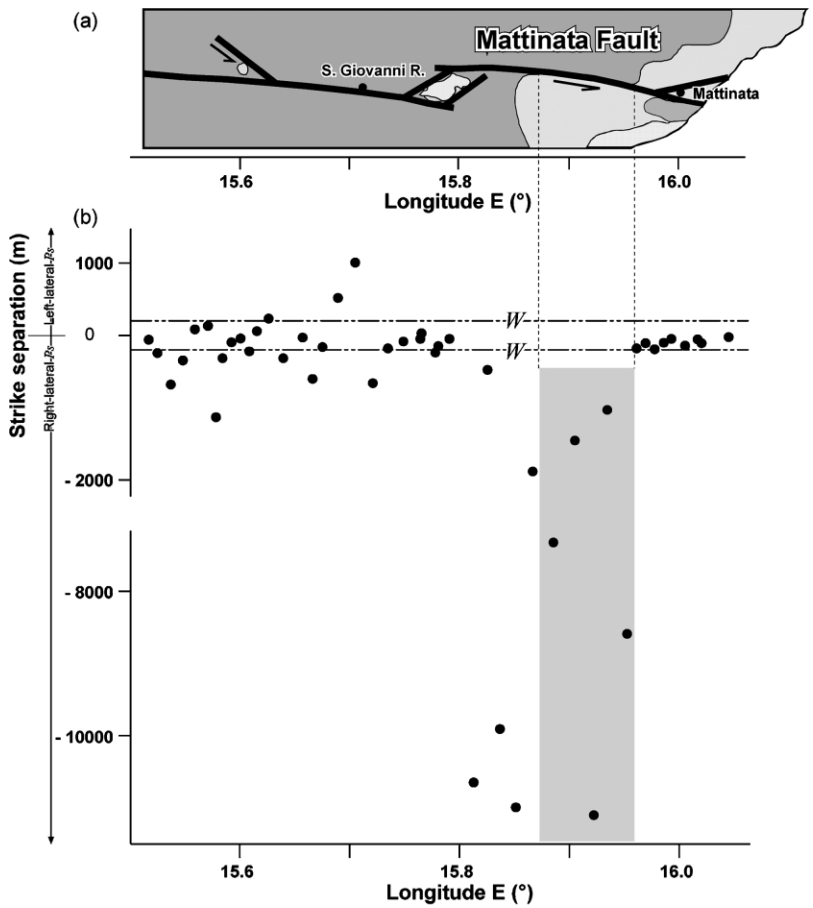

Fig. 10. (a) Geological sketch of the Mattinata Fault area (see Fig. 7 for legend). (b) *Ps* vs. longitude diagram for the Mattinata Fault. *Ps* values are computed from the dataset in Table 1 (Appendix B). Positive ordinates are for left-lateral separations, negative ordinates are for right-lateral separations. Note discontinuity on the negative ordinate scale. *W* (= 200 m) is the Mattinata Fault zone width and may be taken as the resolution limit. Shading in the diagram indicates the *Ps* negative highest values, which correspond in longitude to the area where a right-lateral strike separation can be appreciated on maps (Fig. 7) along the Mattinata Fault.

Table 1
Georeferenced list of data used for the computation of *Ps* along the Mattinata Fault (see Fig. 10b). Note that 'id' is the datum identification number; 'fault azimuth' and 'average cleavage azimuth' are computed from north to east when positive and from north to west when negative; '*Ps*' is positive when left-lateral and negative when right-lateral

Id	Longitude E (°)	Latitude N (°)	Fault azimuth (°)	Average cleavage azimuth (°)	Average cleavage spacing 10^{-2} (m)	Average stylolite amplitude 10^{-3} (m)	*Dn* (m)	α (°)	β (°)	γ (°)	*Ps* (m)
1	15.5181	41.7121	−81.6	−41	18	1	8.1	40	8.1	50	−50.1
2	15.5251	41.7112	−86.4	−46	31	3	13.5	40	3.1	50	−237.9
3	15.5364	41.7106	−88.4	−48	22	2	12.8	40	1.1	50	−655.9
4	15.5483	41.7102	87.3	−53	21	4	24.5	40	3.9	50	−338.8
5	15.5596	41.7107	84.0	−56	29	2	9.9	40	173.1	50	90.1
6	15.5707	41.7115	87.7	−53	16	1	9.0	40	176.1	50	139.5
7	15.5784	41.7118	−88.4	−51	19	3	21.8	37	1.1	53	−1118.9
8	15.5844	41.7116	−84.6	−47	23	5	28.5	37	5.1	53	−297.8
9	15.5929	41.7110	−82.5	−43	22	2	12.9	39	7.1	51	−93.1
10	15.5998	41.7103	−76.0	−37	35	2	8.4	39	13.1	51	−29.3
11	15.6079	41.7088	−87.0	−48	37	2	7.9	39	2.1	51	−209.0
12	15.6157	41.7085	82.8	−59	41	3	10.6	39	171.1	51	67.7
13	15.6260	41.7095	88.8	−53	25	2	11.5	39	177.1	51	236.3
14	15.6397	41.7098	−84.1	−45	17	4	29.6	39	5.1	51	−307.7
15	15.6571	41.7070	−63.2	−21	18	3	21.3	42	26.1	48	−24.3
16	15.6660	41.7036	−86.5	−44	17	5	33.7	42	3.1	48	−591.9
17	15.6753	41.7032	81.7	−57	21	4	23.8	42	8.1	48	−145.8
18	15.6890	41.7048	88.4	−47	23	5	25.2	45	177.1	45	522.6
19	15.7051	41.7053	86.2	−49	24	3	15.7	45	179.1	45	1015.1
20	15.7206	41.7061	−88.1	−43	20	2	12.9	45	1.1	45	−658.9
21	15.7351	41.7057	−86.1	−41	28	2	9.4	45	3.1	45	−164.1
22	15.7489	41.7048	−78.9	−33	27	4	18.2	45	11.1	45	−74.5
23	15.7643	41.7024	−80.0	−35	19	1	7.0	45	9.1	45	−36.7
24	15.7803	41.7003	−70.5	−30	16	4	30.6	40	10.1	50	−146.1
25	15.7908	41.6988	−68.3	−28	19	3	20.9	40	21.1	50	−36.6
26	15.7650	41.7025	61.2	−79	21	2	13.3	40	150.1	50	34.3
27	15.7780	41.7237	−86.2	−46	22	2	12.7	40	3.1	50	−223.9
28	15.8126	41.7221	−89.0	−47	21	3	18.6	42	0.1	48	−10640.0
29	15.8253	41.7260	−88.4	−46	45	3	9.3	42	1.1	48	−475.9
30	15.8365	41.7254	−89.7	−47	38	5	17.3	42	0.1	48	−9896.5
31	15.8508	41.7236	−89.5	−47	27	4	19.2	42	0.1	48	−10983.5
32	15.8665	41.7214	−88.3	−48	16	5	36.5	40	1.1	50	−1870.3
33	15.8847	41.7201	−89.5	−49	11	1	12.8	40	0.1	50	−7323.1
34	15.9043	41.7196	90.5	−50	22	5	28.3	40	1.1	50	−1450.1
35	15.9216	41.7182	−89.8	−50	21	3	19.4	39	0.1	51	−11099.6
36	15.9339	41.7168	−90.0	−51	27	4	20.0	39	1.1	51	−1025.4
37	15.9522	41.7148	−89.5	−50	28	5	15.0	39	0.1	51	−8582.2
38	15.9612	41.7139	−81.6	−47	20	4	27.6	34	8.1	56	−175.3
39	15.9684	41.7130	−81.6	−47	19	2	15.8	34	8.1	56	−100.4
40	15.9767	41.7121	−82.3	−38	18	4	26.2	44	7.1	46	−185.0
41	15.9856	41.7112	−87.1	−43	23	4	21.3	44	11.1	46	−87.9
42	15.9919	41.7103	−68.2	−24	21	5	27.7	44	21.1	46	−45.0
43	16.0034	41.7069	−84.1	−37	20	2	12.4	47	5.1	43	−125.6
44	16.0160	41.7059	−77.4	−30	26	3	14.1	47	12.1	43	−50.6
45	16.0192	41.7039	−77.0	−30	24	5	23.5	47	12.1	43	−84.4
46	16.0447	41.6993	−74.1	−27	21	1	6.2	47	15.1	43	−16.3

Appendix A. Estimate of equation parameters along the Mattinata Fault

We subdivided the Mattinata Fault trace as mapped on the 1:100,000 maps after Servizio Geologico d'Italia (1965, 1970) into 46 segments. For each segment we assessed α, β and *Dn* in order to compute *Sl* and *Ps* associated with each of the 46 fault segments.

1. We computed the α angle as the angular distance from the fault segment, as extracted from Servizio Geologico d'Italia (1965, 1970), to the average cleavage azimuth in that area, as extracted from statistic analysis of Salvini et al. (1999).
2. We computed the β angle as the angular distance from the fault segment, as extracted from Servizio Geologico d'Italia (1965, 1970), to the average

bedding azimuth (i.e. original data collected for this work) in that area.

3. *Dn* can be inferred through the estimate of material removed by pressure solution along cleavage surfaces by using geometric and/or chemical methods (e.g. Stockdale, 1926; Gratier, 1983; Mitra and Yonkee, 1985; Groshong, 1988; Protzman and Mitra, 1990; Wright and Henderson, 1992). For each fault segment, we computed *Dn* according to geometric methods, by comparing the average stylolite amplitude along cleavage surfaces (i.e. original data collected for this work) with the average cleavage spacing in the same area, as extracted from statistic analysis of Salvini et al. (1999). Our results are consistent with indications for estimates of shortening across cleavage surfaces by Alvarez et al. (1978) and Alvarez and Engelder (1982), based on the morphology of cleavage profile.

Appendix B. List of data used for the application to the Mattinata Fault

See Table 1.

References

Aiello, G., de Alteriis, G., 1991. Il margine adriatico della Puglia: fisiografia ed evoluzione terziaria. Memorie della Società Geologica Italiana 47, 197–212.

Alvarez, W., Engelder, T., 1982. Solution cleavage and estimates of shortening, Umbrian Apenines. In: Borradaile, G.J., Bayly, M.B., Powell, C.M. (Eds.), Atlas of Deformational and Metamorphic Rock Fabrics, Springer-Verlag, Berlin, pp. 178–179.

Alvarez, W., Engelder, T., Geiser, P.A., 1978. Classification of solution cleavage in pelagic limestones. Geology 6, 263–266.

Anzidei, M., Baldi, P., Casula, G., Crespi, M., Riguzzi, F., 1996. Repeated GPS surveys across the Ionian Sea: evidence of crustal deformations. Geophysical Journal International 127, 257–267.

Aydin, A., 1978. Small faults formed as deformation bands in sandstone. Pure and Applied Geophysics 116, 913–930.

Aydin, A., 1988. Discontinuities along thrust faults and the cleavage duplexes. In: Mitra, G., Wojtal, S. (Eds.), Geometries and Mechanics of Thrusting. Geological Society of America Special Publication 222, pp. 223–232.

Aydin, A., Johnson, A.M., 1978. Development of faults as zones of deformation bands and as slip surfaces in sandstone. Pure and Applied Geophysics 116, 931–942.

Bell, T.H., 1978. The development of slaty cleavage across the Nackara Arc of the Adelaide geosyncline. Tectonophysics 51, 171–201.

Bertotti, G., Casolari, E., Picotti, V., 1999. The Gargano Promontory: a Neogene contractional belt within the Adriatic plate. Terra Nova 11, 168–173.

Beutner, E.C., Charles, E.G., 1985. Large volume loss during cleavage formation, Hamburg sequence, Pennsylvania. Geology 13, 803–805.

Billi, A., 2000. Stili e processi deformativi nell'avampaese apulo. Ph.D. thesis, "Roma Tre" University of Rome.

Billi, A., Salvini, F., 2000. Sistemi di fratture associati a faglie in rocce carbonatiche: nuovi dati sull'evoluzione tettonica del Promontorio del Gargano. Bollettino della Società Geologica Italiana 119, 237–250.

Billi, A., Salvini, F., 2001. Fault-related solution cleavage in exposed carbonate reservoir rocks in the southern Apennines, Italy. Journal of Petroleum Geology 24, 147–169.

Borgomano, J.R.F., 2000. The Upper Cretaceous carbonates of the Gargano and Murge region, southern Italy: a model of platform-to-basin transition. American Association of Petroleum Geologists Bulletin 84, 1561–1588.

Bosellini, A., Neri, C., Luciani, V., 1993a. Guida ai carbonati cretaceo–eocenici di scarpata e bacino del Gargano. Annali dell'Università di Ferrara, Scienze della Terra 4, 1–77.

Bosellini, A., Neri, C., Luciani, V., 1993b. Platform margin collapses and sequence stratigraphic organization of carbonate slopes: Cretaceous–Eocene, Gargano Promontory, Southern Italy. Terra Nova 5, 282–297.

Bosellini, A., Morsilli, M., Neri, C., 1999. Long-term event stratigraphy of the Apulia platform margin (Upper Jurassic to Eocene, Gargano, Southern Italy). Journal of Sedimentary Research 69, 1241–1252.

Casolari, E., Negri, A., Picotti, V., Bertotti, G., 2000. Neogene stratigraphy and sedimentology of the Gargano Promontory (southern Italy). Eclogae Geologicae Helvetiae 93, 7–23.

Chilovi, C., De Feyter, A.J., Pompucci, A., 2000. Wrench zone reactivation in the Adriatic block: the example of the Mattinata Fault system (SE Italy). Bollettino della Società Geologica Italiana 119, 3–8.

Conybeare, C.E.B., 1949. Stylolites in Precambrian quartzite. Journal of Geology 57, 83–85.

Davidson, S.G., Anastasio, D.J., Bebout, G.E., Holl, J.E., Hedlund, C.A., 1998. Volume loss and metasomatism during cleavage formation in carbonate rocks. Journal of Structural Geology 20, 707–726.

de Alteriis, G., 1995. Different foreland basins in Italy: examples from the central and southern Adriatic Sea. Tectonophysics 252, 349–373.

de Dominicis, A., Mazzoldi, G., 1987. Interpretazione geologico-strutturale del margine orientale della piattaforma apula. Memorie della Società Geologica Italiana 38, 163–176.

Dennis, J.G., 1967. International tectonic dictionary. American Association of Petroleum Geologists Memoirs 7.

Doglioni, C., Mongelli, F., Pieri, P., 1994. The Puglia uplift (SE Italy). an anomaly in the foreland of the Apenninic subduction due to buckling of a thick continental lithosphere. Tectonics 13, 1309–1321.

Durney, D.W., 1972. Solution-transfer, an important geological deformation mechanism. Nature 235, 315–317.

Durney, D.W., Kisch, H.J., 1994. A field classification and intensity scale for first-generation cleavages. AGSO Journal of Australian Geology & Geophysics 15, 257–295.

Engelder, T., 1984. The role of pore water circulation during the deformation of foreland fold and thrust belts. Journal of Geophysical Research 89, 4319–4325.

Engelder, T., Geiser, P.A., 1979. The relationship between pencil cleavage and lateral shortening within the Devonian section of the Appalachian Plateau, New York. Geology 7, 460–464.

Favali, P., Funiciello, R., Mattietti, G., Mele, G., Salvini, F., 1993. An active margin across the Adriatic Sea (central Mediterranean Sea). Tectonophysics 219, 109–117.

Finetti, I., Del Ben, A., 1986. Geophysical study of the Tyrrhenian opening. Bollettino di Geofisica Teorica ed Applicata 28, 75–155.

Finetti, I., Bricchi, G., Del Ben, A., Pipan, A., Xuan, Z., 1987. Geophysical study of the Adria plate. Memorie della Società Geologica Italiana 40, 335–344.

Funiciello, R., Montone, P., Salvini, F., Tozzi, M., 1988. Caratteri strutturali del Promontorio del Gargano. Memorie della Società Geologica Italiana 41, 1235–1243.

Gambini, R., Tozzi, M., 1996. Tertiary geodynamic evolution of the Southern Adria microplate. Terra Nova 8, 336–340.

Gratier, J.P., 1983. Estimation of volume changes by comparative chemical analyses in heterogeneously deformed rocks (folds with mass transfer). Journal of Structural Geology 5, 329–339.

Gray, M.B., Mitra, G., 1993. Migration of deformation fronts during progressive deformation: evidence from detailed structural studies in

the Pennsylvania Anthracite region, USA. Journal of Structural Geology 15, 435–449.
Graziano, R., 1999. The Early Cretaceous drowning unconformities of the Apulia carbonate platform (Gargano Promontory, southern Italy): local fingerprints of global palaeoceanographic events. Terra Nova 11, 245–250.
Graziano, R., 2000. The Aptian–Albian of the Apulia carbonate platform (Gargano Promontory, southern Italy): evidence of the palaeoceanographic and tectonic controls on the stratigraphic architecture of the platform margin. Cretaceous Research 21, 107–126.
Groshong, R.H., 1975a. "Slip" cleavage caused by pressure solution in a buckle fold. Geology 3, 411–413.
Groshong, R.H., 1975b. Strain, fractures, and pressure solution in natural single-layer folds. Geological Society of America Bulletin 86, 1363–1376.
Groshong, R.H., 1976. Strain and pressure solution in the Martinsburg slate, Delaware Water Gap, New Jersey. American Journal of Science 276, 1131–1146.
Groshong, R.H., 1988. Low-temperature deformation mechanisms and their interpretation. Geological Society of America Bulletin 100, 1329–1360.
Groshong, R.H., 1999. 3-D Structural Geology, Springer-Verlag, Berlin.
Guerricchio, R., 1983. Strutture tettoniche di compressione nel Gargano di elevato interesse applicativo evidenziate da immagine da satellite. Geologia Applicata e Idrogeologia 18, 491–505.
Guerricchio, R., 1986. Esempi di bacini di pull apart nel Gargano (Puglia settentrionale). Geologia Applicata e Idrogeologia 21, 25–36.
Guerricchio, A., Pierri, P., 1998. Sismicità del territorio di San Giovanni Rotondo (FG). Geologia Tecnica & Ambientale 6/3, 25–39.
Hobbs, B.E., Means, W.D., Williams, P.F., 1976. An Outline of Structural Geology, John Wiley and Sons, New York.
Markley, M., Wojtal, S., 1996. Mesoscopic structure, strain and volume loss in folded cover strata, Valley and Ridge Province, Maryland. American Journal of Science 296, 23–57.
Marshak, S., Mitra, G., 1988. Basic Methods of Structural Geology, Prentice Hall, New Jersey.
Masse, J.-P., Luperto Sinni, E., 1987. A platform to basin transition model: the lower Cretaceous carbonates of the Gargano massif (southern Italy). Memorie della Società Geologica Italiana 40, 99–108.
McNaught, M.A., Mitra, G., 1996. The use of finite strain data in constructing a retrodeformable cross-section of the Meade thrust sheet, southeastern Idaho, USA. Journal of Structural Geology 18, 573–583.
Mimran, Y., 1977. Chalk deformation and large-scale migration of calcium carbonate. Sedimentology 24, 333–360.
Mitra, G., 1994. Strain variation in thrust sheets across the Sevier fold-and-thrust belt (Idaho–Utah–Wyoming): implications for section restoration and wedge taper evolution. Journal of Structural Geology 16, 585–602.
Mitra, G., Yonkee, W.A., 1985. Relationship of spaced cleavage to folds and thrusts in the Idaho–Utah–Wyoming thrust belt. Journal of Structural Geology 7, 361–373.
Mitra, G., Yonkee, W.A., Gentry, D.J., 1984. Solution cleavage and its relationship to major structures in the Idaho–Utah–Wyoming thrust belt. Geology 12, 354–358.
Mollema, P.N., Antonellini, M.A., 1996. Compaction bands: a structural analog for anti-mode I cracks in aeolian sandstone. Tectonophysics 267, 209–228.
Morsilli, M., Bosellini, A., 1997. Carbonate facies zonation of the Upper Jurassic–Lower Cretaceous Apulia platform margin (Gargano Promontory, Southern Italy). Rivista Italiana di Paleontologia e Stratigrafia 103, 193–206.
Nickelsen, R.P., 1966. Fossil distortion and penetrative rock deformation in the Appalachian plateau, Pennsylvania. Journal of Geology 74, 924–931.
Nickelsen, R.P., 1972. Attributes of rock cleavage in some mudstones and limestones of the Valley and Ridge Province, Pennsylvania. Pennsylvania Academy of Science 46, 107–112.
Nickelsen, R.P., 1986. Cleavage duplexes in the Marcellus Shale of the Appalachian foreland. Journal of Structural Geology 8, 361–371.
Ortolani, F., Pagliuca, S., 1987. Tettonica transpressiva nel Gargano e rapporti con le catene Appenninica e Dinarica. Memorie della Società Geologica Italiana 38, 205–224.
Ortolani, F., Pagliuca, S., 1988. Il Gargano (Italia Meridionale): un settore di "avampaese" deformato tra le catene appenninica e dinarica. Congresso della Società Geologica Italiana 74, A411–A417.
Peacock, D.C.P., Sanderson, D.J., 1995. Pull-aparts, shear fractures and pressure solution. Tectonophysics 241, 1–13.
Peacock, D.C.P., Fisher, Q.J., Willemse, E.M.J., Aydin, A., 1999. The relationship between faults and pressure solution seams in carbonate rocks and the implications for fluid flow. In: Jones, G., Fisher, Q.J., Knipe, R.J. (Eds.), Faulting, Fault Sealing and Fluid flow in Hydrocarbon Reservoirs. Geological Society Special Publication 147, pp. 105–115.
Protzman, G.M., Mitra, G., 1990. Strain fabric associated with the Meade thrust sheet: implications for cross-section balancing. Journal of Structural Geology 12, 403–417.
Ramsay, J.G., Wood, D.S., 1972. The geometric effects of volume change during deformation processes. Tectonophysics 16, 263–277.
Ricchetti, G., Pieri, P. (Eds.), 1999. Guide Geologiche Regionali a cura della Società Geologica Italiana, Puglia e Monte Vulture. BE-MA editrice, Roma.
Roy, A.B., 1978. Evolution of slaty cleavage in relation to diagenesis and metamorphism: a study from Hunsruckschiefer. Geological Society of America Bulletin 89, 1775–1785.
Salvini, F., Billi, A., Wise, D.U., 1999. Strike-slip fault-propagation cleavage in carbonate rocks: the Mattinata Fault zone, Southern Apennines, Italy. Journal of Structural Geology 21, 1731–1749.
Sellwood, B.W., 1996. Shallow-marine carbonate environments. In: Reading, H.G., (Ed.), Sedimentary Environments and Facies, Blackwell Scientific Publications, Oxford, pp. 283–342.
Servizio Geologico d'Italia, 1965. Carta Geologica D'Italia, scala 1:100.000, Foglio 164 "Monte S. Angelo". Servizio Geologico d'Italia Map 164, scale 1:100,000.
Servizio Geologico d'Italia, 1970. Carta Geologica D'Italia, scala 1:100.000, Foglio 156 "S. Marco in Lamis". Servizio Geologico d'Italia Map 159, scale 1:100,000.
Sharpe, D., 1847. On slaty cleavage. Geological Society of London Quarterly Journal 3, 74–105.
Stockdale, P.B., 1926. The stratigraphic significance of solution in rocks. Journal of Geology 34, 399–414.
Tramontana, M., Morelli, D., Colantoni, P., 1995. Tettonica plio-quaternaria del sistema sud-garganico (settore orientale) nel quadro evolutivo dell'Adriatico centro-meridionale. Studi Geologici Camerti, Volume Speciale 1995/2, 467–473.
van der Pluijm, B.A., Marshak, S., 1997. Earth Structure: an Introduction to Structural Geology and Tectonics, McGraw-Hill, New York.
Whitaker, A.E., Bartholomew, M.J., 1999. Layer parallel shortening: a mechanism for determining deformation timing at the junction of the central and southern Appalachians. American Journal of Science 299, 238–254.
Willemse, E.M.J., Peacock, D.C.P., Aydin, A., 1997. Nucleation and growth of strike-slip faults in limestones from Somerset, UK. Journal of Structural Geology 19, 1461–1477.
Wintsch, R.P., Kvale, C.M., Kisch, H.D., 1991. Open-system, constant volume development of slaty cleavage, and strain-induced replacement reactions in the Martinsburg Formation, Lehigh Gap, Pennsylvania. Geological Society of America Bulletin 103, 916–927.
Wise, D.U., Vincent, R.J., 1965. Rotation axis method for detecting conjugate planes in calcite petrofabric. American Journal of Science 263, 289–301.
Wojtal, S., 1986. Deformation within foreland thrust sheets by populations of minor faults. Journal of Structural Geology 8, 341–360.

Wojtal, S., Mitra, G., 1986. Strain hardening and strain softening in fault zones from foreland thusts. Geological Society of America Bulletin 97, 674–687.

Wright, T.O., Henderson, J.R., 1992. Volume loss during cleavage formation in the Meguma Group, Nova Scotia, Canada. Journal of Structural Geology 14, 281–290.

Wright, T.O., Platt, L.B., 1982. Pressure dissolution and cleavage in the Martinsburg Shale. American Journal of Science 282, 122–135.